Research Article | Vol. 32, No. 24 / 18 Nov 2024 / Optics Express 43407
Optics EXPRESS

GaAs-based antenna-coupled field effect transistors as direct THz detectors across a wide frequency range from 0.2 to 29.8 THz

Rahul Yadav,[1,2,*] Florian Ludwig,[3] Fahd Rushd Faridi,[1] J. Michael Klopf,[4] Hartmut G. Roskos,[3] Andreas Penirschke,[2] and Sascha Preu[1]

[1]Terahertz Devices and Systems, Technical University of Darmstadt, 64283 Darmstadt, Germany
[2]High Frequency Technology, Mittelhessen University of Applied Sciences, 61169 Friedberg, Germany
[3]Institute of Physics, Johann Wolfgang Goethe University, 60438 Frankfurt am Main, Germany
[4]Institute of Radiation Physics, Helmholtz-Zentrum Dresden-Rossendorf, 01328 Dresden, Germany
[*]yadav@imp.tu-darmstadt.de

Abstract: High-power coherent terahertz (THz) radiation from accelerator facilities such as free-electron lasers (FELs) is frequently used in pump-probe experiments where the pump or probe (or both) signals are intense THz pulses. Detectors for these applications have unique requirements that differ from those of low-power table-top systems. In this study, we demonstrate GaAs antenna-coupled field effect transistors (FETs) as a direct THz detector operating across a broad frequency spectrum ranging from 0.2 THz to 29.8 THz. At approximately 0.5 THz, the maximum current responsivity ($\mathfrak{R}_I$) of 0.59 mA/W is observed, signifying a noise equivalent power (NEP) of 2.27 nW/$\sqrt{Hz}$. We report an empirical roll-off of f^{-3} for an antenna-coupled GaAs TeraFET detector. Still, NEP of 0.94 μW/$\sqrt{Hz}$ and a current responsivity $\mathfrak{R}_I = 1.7\mu$A/W is observed at 29.8 THz, indicating that with sufficient power the FET can be used from sub-mm wave to beyond far-infrared frequency range. Current and voltage noise floor of the characterized TeraFET is 2.09 pA and 6.84 μV, respectively. This characteristic makes GaAs FETs more suitable for applications requiring higher frequencies, ultra-broadband capabilities and robustness in the THz domain, such as beam diagnostics and alignment at particle accelerators.

Published by Optica Publishing Group under the terms of the Creative Commons Attribution 4.0 License. Further distribution of this work must maintain attribution to the author(s) and the published article's title, journal citation, and DOI.

1. Introduction

Prodigious evolution of Terahertz (THz) devices and systems over the last decades [1–4] has been an outstanding achievement towards bridging the "THz Gap" between the electronics and optics domain of electromagnetic spectrum. Interesting applications of THz technologies [1] are the core driving forces behind the exponential development of THz components. In addition to applied research in commercially potential relevant areas like security [5,6] and non-destructive testing [7–9] an important application in fundamental science is diagnostics and synchronization [10–12] of THz beams at particle accelerator facilities. These facilities require fast, robust, broadband and stable detectors [13]. Coherent detection schemes can measure ps-scale pulses and are highly sensitive but they can either be used for single pulse measurements only or require phase-locking with the source. Direct detectors rectify the incident THz signal and do not require phase-locking with the source. Direct thermal detectors, such as Golay cells, bolometers, and pyroelectric detectors [14–16] can spatially trace the THz signal from the source; however, they are only able to rectify the pulse on > 100 ps time scales [17] and often only on the μs to ms time scale, which is insufficient for accelerator facilities that typically provide pulse lengths below 50 ps.

#534393 https://doi.org/10.1364/OE.534393
Journal © 2024 Received 1 Jul 2024; revised 15 Sep 2024; accepted 15 Sep 2024; published 14 Nov 2024

Optics EXPRESS

Plasma wave-based direct THz detectors such as high electron mobility transistors (HEMTs) [10,18–20] as well as Schottky diodes [12,21] with picosecond (ps) scale pulse detection are at least two orders of magnitude faster than the aforementioned thermal detectors. Rectification in FETs is due to the simultaneous modulation of the carrier concentration in the transistor channel, typically a two-dimensional electron gas (2DEG), by a THz bias, $en^{(2D)} = cU_{THz}$, and the carrier velocity $v = \mu E_{THz} \sim U_{THz}$, where μ is the carrier mobility and c is the gate-channel capacitance per unit area. A THz bias is often generated by an attached on-chip antenna that receives an incoming THz signal. The details on the rectification effect can be found elsewhere [10,11,22,26,27]. The incident THz signal excites a plasma wave, which is rectified in the channel producing a drain-source current (or voltage) proportional to the incident signal. This current is processed via post-detection electronics such as a lock-in amplifier or a fast oscilloscope [11]. The entire electron population in the channel is collectively excited by the plasma wave, which is regarded as a Fermi fluid [4] and is commonly known as a two-dimensional electron gas (2DEG). The rectified signal is a consequence of the non-linear self-mixing properties of the collective excitations of the two-dimensional electron gas (2DEG) in the FET channel termed plasma waves, which are excited by incident THz radiation. The theory of electron motion in 2DEG is explained in the outstanding work of Dyakonov and Shur [23,24].

Antenna-coupled THz FETs based on various III-V technologies such as GaAs [10,11], GaN [19], Si CMOS [16] and Graphene [20,25] are widely developed in the community. These are commonly known as TeraFETs. GaAs TeraFETs are excellently suited for diagnostics and synchronization at free electron laser (FEL) facilities because of their high electron mobility and sheet charge concentrations. Moreover, because of their ultra-wide operation [10,11], they eliminate the need to switch detectors for different FEL operation frequencies, facilitating experiments [26]. They are inexpensive and easy to handle because of their small size and ability to function at room temperature.

In this study, we investigate the THz frequency dependency of the response of GaAs TeraFETs within the frequency range from 0.2 to 29.8 THz by using two different sources, namely, a PIN-diode photomixer driven by continuous wave (CW) Laser and a FEL. This paper is divided into five sections. The motivation, introduction and state-of-the-art of similar technologies are described briefly in section I. Section II focuses on the device fabrication and packaging techniques. Section III explains the experimental setup and methods used for the characterization of the detector. The results and discussion are presented in section IV, followed by the section V highlighting the conclusions of this study.

2. GaAs TeraFET layout and detector packaging

Figure 1(a) shows a schematic of the fabricated device structure. It contains a semi-insulating (SI) low-temperature grown GaAs substrate of 500 μm thickness. Two-dimensional electron gas (2DEG) is formed at the interface of Aluminium Gallium Arsenide (AlGaAs) and GaAs layer. The barrier thickness between the 2DEG and gate contact was only 30 nm.

The GaAs TeraFET with a channel of $4 \times 4\ \mu m^2$ is situated between the electrodes (electrodes are defined as source and drain, which are at a distance of 4 μm end-to-end) of the antenna, as shown in Fig. 1(b). Strong capacitive gate-source coupling (as shown in Fig. 1(a) and (b)) provides an AC short between the source and gate by the presence of a 110 nm thick silicon nitride (Si_3N_4) insulation layer to AC ground the gate. The gate length was 2 μm, where 1 μm is extending on top of the Si_3N_4. The un-gated part between the gate and drain was 2 μm long. A frequency-independent log-spiral antenna is used for the ultra-broadband frequency response of the detector from about 100 GHz up to about 2 THz. Figure 2 shows the radiation impedance of the self-complementary antenna. Theoretically for this type of antenna radiation resistance of $R_A = 72\,\Omega$, whereas the simulations show $R_A = 67 \pm 5\,\Omega$. From the simulations, it is observed that above 3.5 THz the antenna is not efficient anymore as its radiation resistance drops and the

Optics EXPRESS

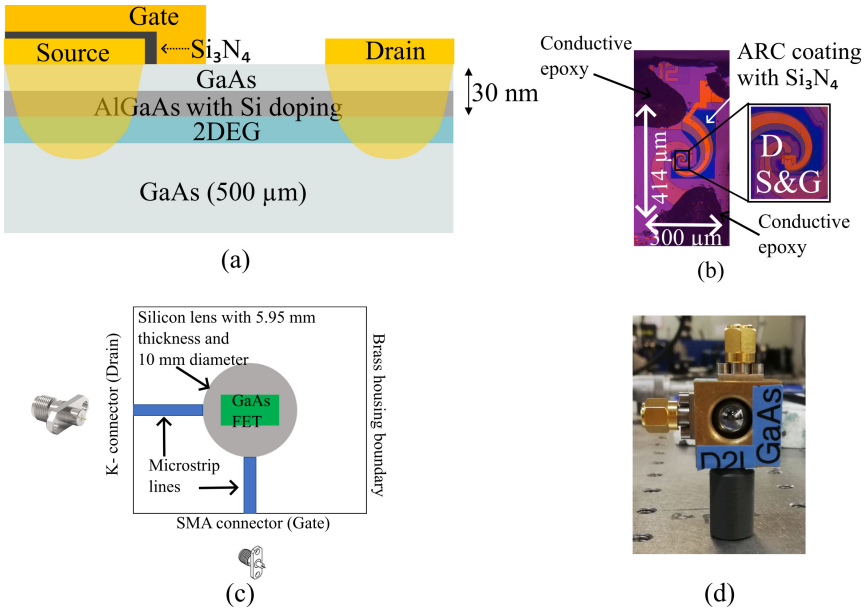

Fig. 1. (a) Depiction of the fabricated device with a capacitive AC short between source and gate, (b) illustration of fabricated log-spiral antenna-coupled FET device with the antenna coupled to source and drain. The inset shows a zoom-in to the active area of $4 \times 4\ \mu m^2$ device showing the gate going over the source terminal, (c) illustration of the device packaging technique (green rectangle denotes GaAs TeraFET device) and (d) packaged GaAs TeraFET.

reactance increases. This is because its inner dimensions, limited by the device size, are too large in relation to the wavelength. Consequently, at higher THz frequencies, the THz wave couples directly with the core electrodes of the detector.

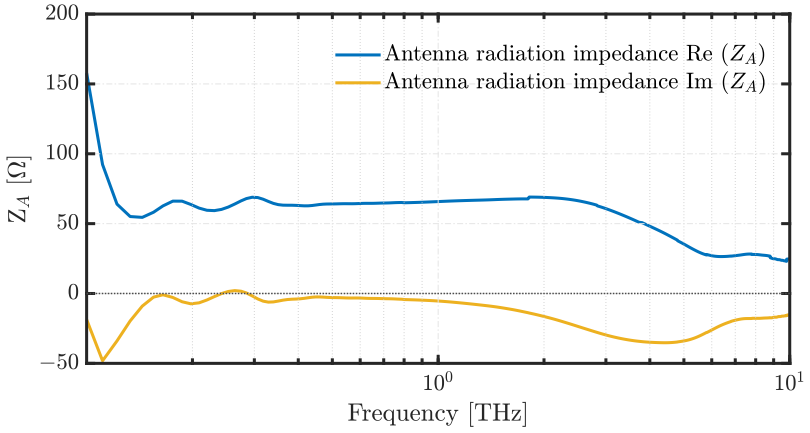

Fig. 2. Simulated radiation impedance of log-spiral antenna of the characterized detector.

Figure 1(c) depicts the packaging technique used for the detector. The GaAs TeraFET device was mounted on a hyper-hemispherical high resistivity float zone silicon (HRFZ-Si) lens. The hyper-hemispherical offset of the lens (R_{hyp}), including the TeraFET substrate, is chosen to

Optics EXPRESS

approximate the aplanatic condition [28] as

$$R_{hyp} = r \cdot (1 + \frac{1}{n_1}) - s \cdot \frac{n_1}{n_2} \quad (1)$$

where, r is the lens radius and n is the refractive index. For a $s = 500$ μm thick GaAs substrate with $n_2 = 3.6$ the hyper-hemisphericity of the silicon lens ($n_1 = 3.416$) is chosen as R_{hyp}=5.95 mm for $r = 5$ mm. The rectified signal is read out between the drain and source ports, a K-type end-launch connector with an RF bandwidth up to 40 GHz is used. The source-gate terminal was connected by a standard SMA connector as it is only used for DC biasing of the TeraFET to the working point. The device was packaged inside a brass housing, as shown in Fig. 1(d). The brass housing provides shielding from parasitic electromagnetic coupling including RF signals, such as those originating from the repetition rate of the FEL, in this example 13 MHz.

3. Experimental setup and techniques

Figure 3(a) illustrates the experimental table-top setup of the Toptica TeraScan 1550 CW system used to characterize the detector from 0.2 and 1.2 THz. A PIN-diode photomixer (HHI) driven by a set of two continuous wave lasers operating around 1550 nm was used as the transmitter. It produces a power of 1.2 and 0.065 μW at 0.5 and 1 THz, respectively. The refrence power of pin-diode was measured using a Golay cell calibrated to a Thomas Keating power meter. The rectified signal from the THz detector is fed into a trans-impedance amplifier (PDA-S, TEM Messtechnik) with a gain of 3.3×10^6 V/A, followed by a lock-in amplifier (Toptica digital control electronics DLC smart).

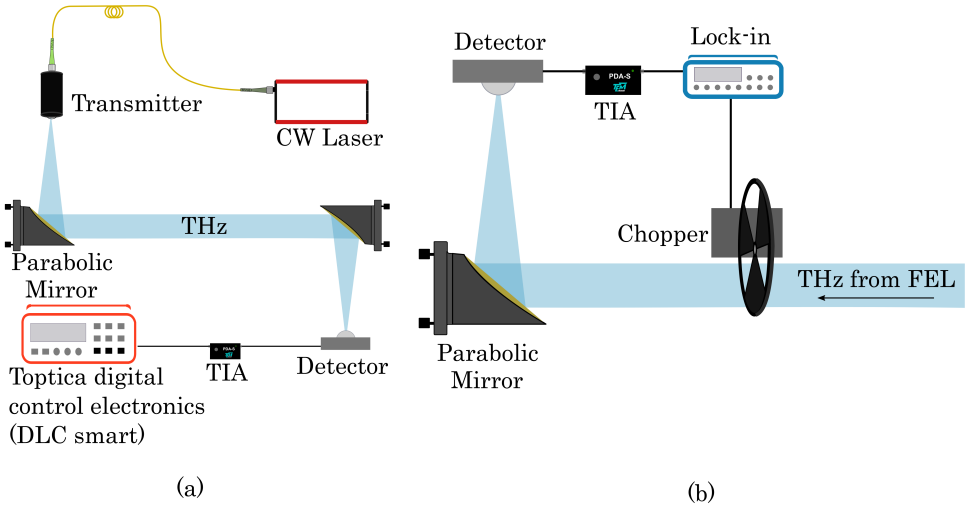

Fig. 3. Schematic of (a) the experimental setup used for table-top characterization and (b) the experimental setup used during FEL beamtime at HZDR.

Further studies were conducted at the FEL facility FELBE at the Helmholtz Zentrum Dresden-Rossendorf, Dresden, Germany, in order to characterize the TeraFET for its functioning limits, as well as its responsivity and behavior with respect to high power levels, particularly at several THz.

The main advantage of employing the FEL for characterization is that the detector can be tested over a very wide range of intensities because of its huge power and correspondingly high pulse energy (up to 2 μJ) as compared to table-top systems. Coherent electromagnetic radiation in the 5–250 μm range, encompassing the frequency range of 1.2–60 THz, is produced at FELBE by

Optics EXPRESS

two FELs (U37 and U100). 13 MHz repetition rate collimated pulses are delivered by both FELs. An extensive variety of parameters for testing and evaluation of the GaAs TeraFET THz detectors are offered by the ability to fully control the wavelength and power of the FEL beam. The detector is characterized at eight frequency points: 3.08, 4.06, 4.84, 5.56, 12.24, 15.35, 24.9 and 29.8 THz. The frequency points were carefully chosen to avoid water vapor absorption lines and the Reststrahlenband (~7.5 to 10 THz) of the GaAs substrate. The average power of the FELBE FEL depends on the wavelength but can reach several tens of watts at most wavelengths, several orders of magnitude greater than the average power of typical table-top THz sources. Since the TeraFET detectors are may be destroyed by a few watts of power, a set of step attenuators in the beam line are applied to control the power delivered to the measurement site. The power applied to the TeraFETs for these measurements varies from 0.1 to 4.6 mW depending on the frequency. We maintain the THz power at a low level to keep the device well below saturation, prioritizing its protection for subsequent measurements.

Figure 3(b) shows the schematic of the setup configuration with FEL as source. The GaAs TeraFET detector was characterized in the photo-current read-out mode. The incoming THz signal from the FEL was modulated using a chopper at a modulation frequency of 113 Hz. An Ophir Optronics 3A-P-THz sensor was used to measure the power in order to perform calibration. The rectified signal from the GaAs THz detector is first amplified by implementing a trans-impedance amplifier (PDA-S, TEM Messtechnik) with a gain of 3.3×10^6 V/A and then demodulated by a lock-in amplifier (7270 DSP, signal recovery) as shown in Fig. 3(b). The lock-in-amplifier-based detection technique detects all rectifying effects, including those that depend on the temperature changes caused by the strong FEL beam.

4. Results and discussion

Figure 4 shows the linearity results for the experiments performed using FEL as a source at U_{GS} = 0 V with a TIA gain of 3.3×10^6 V/A. The detector was characterized at different FEL power levels. The standard attenuators in-built into FEL beam-line were regulated for delivery of the desired THz power at the optical test bench. At 4.06 THz, the detector shows an unusual behavior even at sub 0.5 mW THz power. From antenna simulation results, at 4.06 THz, the R_A = 47.8 Ω, which might have caused the TeraFET to be in resonance at 4.06 THz and lead to significant increase in response and some minor saturation at the highest investigated FEL power level. At all other frequencies detector shows a linear, unsaturated behavior. The inset of Fig. 4 shows a zoom-in from 0 to 2 mW THz power.

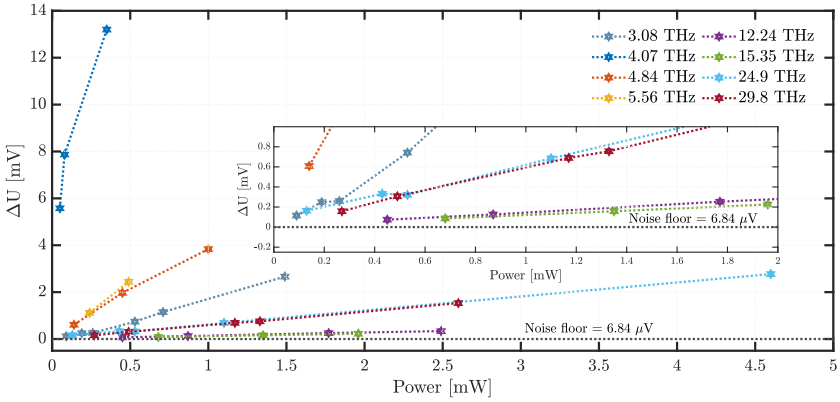

Fig. 4. Linearity characterization of the detector with FEL at U_{GS} = 0 V. Inset shows zoomed-in part from 0 to 2 mW average power.

Optics EXPRESS

The DC characterization (right y-axis) is shown in Fig. 5. At U_{GS}= + 0.3 V, U_{GS}=0 V, and U_{GS}= - 0.30 V , R_{DS} is 5.83 $k\Omega$, 29.93 $k\Omega$, and 53.19 $M\Omega$, respectively. The threshold voltage U_{GS}^{th} is approximately at - 0.2 V, as shown by the strong increase of device resistance (R_{DS}) for lower U_{GS} voltages. As the detector was characterized in photo-current read-out mode, we present the current responsivity of the detector. The responsivity signifies detector output signal with respect to incident/coupled THz power to it and when the detector is operated in current read-out mode, it is expressed as current responsivity ($\mathfrak{R}_I$). The current responsivity $\mathfrak{R}_I$ is calculated as [4]

$$\mathfrak{R}_I = \frac{\Delta U / P_{THz}}{3.3 \times 10^6 V/A} \tag{2}$$

ΔU is the measured rectified voltage, P_{THz} is the incident average THz power and 3.3×10^6 V/A is the TIA gain. Therefore, $\mathfrak{R}_I$ is the intrinsic response of the TeraFET.

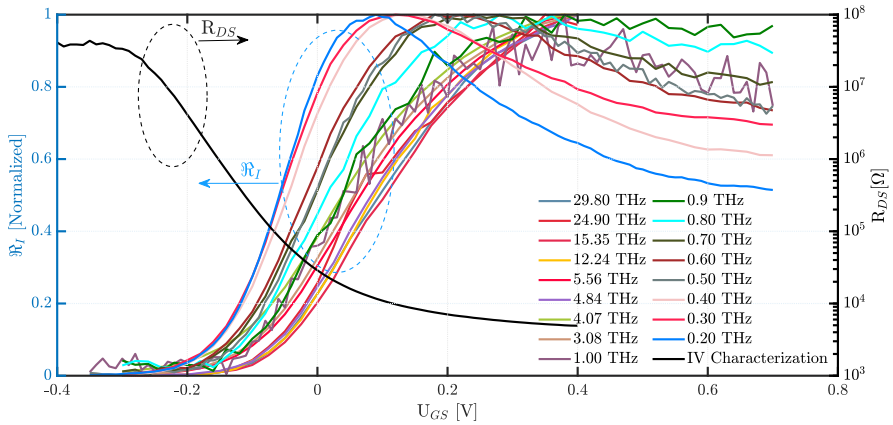

Fig. 5. Left y-axis: normalized current responsivity of the detector and right y-axis: DC characterization of the detector with respect to U_{GS} bias (shown by black solid line).

Figure 5 shows the combined table-top and FELBE THz current responsivity (left y-axis) of the detector with respect to U_{GS} bias, normalized to its respective peak value. Starting from the threshold bias of -0.2 V, increasing the U_{GS} bias leads to an increase of the current responsivity to 0.34 mA/W at U_{GS} = 0 V (at 0.2 THz). The maximum $\mathfrak{R}_I$ of 0.59 mA/W is observed at U_{GS} = 0.18 V at 0.5 THz. As the frequency increases, the maximum peak of $\mathfrak{R}_I$ shifts towards a more positive U_{GS} bias . For U_{GS} = 0 V at 29.8 THz $\mathfrak{R}_I$ = 0.42 μA/W is observed. For the FELBE measurements, the maximum $\mathfrak{R}_I$ is observed close to U_{GS} = 0.4 V or even slightly beyond. The rightward shift of the maximum normalized $\mathfrak{R}_I$ might be due to thermo-electric contributions that influence the charge carrier density in the gated area when gate bias is applied. This signifies the presence of thermo-electric effects along with the Dyakonov-Shur rectification mechanism at higher frequencies. In the following, we use U_{GS} = 0.3 V as a compromise between high frequency and low frequency optimum bias to compare the detector response at different frequencies and determine its roll-off.

Figures 6(a) and (b) show the detector responsivity and noise equivalent power (NEP), respectively from 0.2 to 29.8 THz at U_{GS} = 0.3 V. NEP is defined as the ratio of the detector noise (current or voltage) spectral density in 1 Hz bandwidth and the detector responsivity (current or voltage). The ideal NEP of the characterized TeraFET was calculated as [19]

$$NEP = \left(\frac{4k_B T_0}{R_{DS}}\right)^{1/2} \frac{1}{\mathfrak{R}_I} \tag{3}$$

Optics EXPRESS

where, k_B is Boltzmann constant with k_B=1.3810^{-23} J/K, (T_0) is temperature in Kelvin, R_{DS} is source-drain resistance and $\mathfrak{R}_I$ is the calculated current responsivity from the measured data (using Eq. (2)). We determined the noise floor of 6.84 μV (or 2.07 pA using TIA gain of 3.3×10^6 V/A) at a water line at 1.10 THz, where the signal drops into noise. As the lock-in could not lock any more, we indeed reached the noise floor that agreed with the thermal noise floor in Eq. (3). The current noise floor, $\left(\frac{4k_BT_0}{R_{DS}}\right)^{1/2}$ is a device-specific quantity that is independent of the THz frequency. We skipped noise measurements as the beam time at FELBE is strongly restricted.

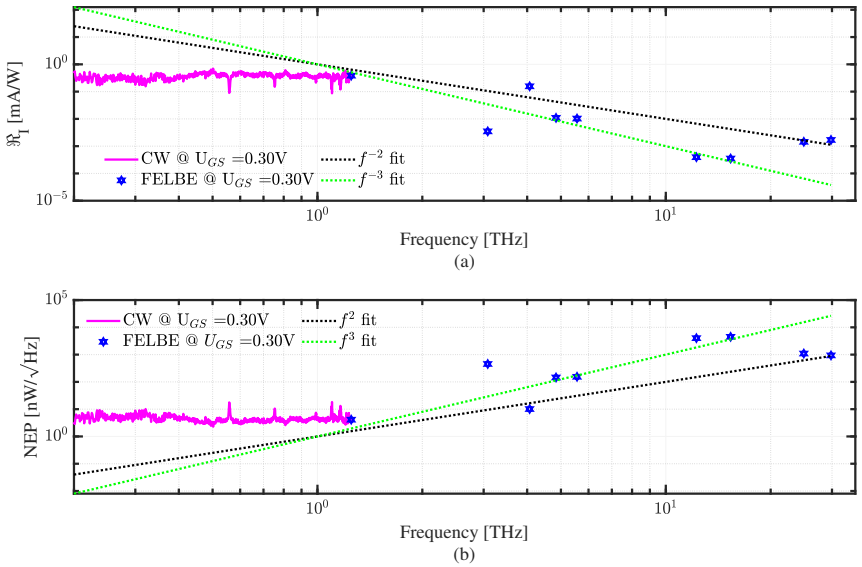

Fig. 6. (a) Current responsivity and (b) NEP of the investigated GaAs TeraFET detector over the frequency range 0.2 to 29.8 THz. Device response at U_{GS} = 0.3 V with CW system and FEL is shown in magenta and blue hexagrams, respectively. Green represents f^{-3} fit for responsivity and f^3 fit for NEP, while dotted line in black represents f^{-2} fit for responsivity and f^2 fit for NEP.

The NEP and $\mathfrak{R}_I$ values are summarized in Table 1. The nearly flat responsivity of the table-top system (from 0.2 THz to 1.2 THz) is inferred empirically. This agrees with the trend of the antenna radiation impedance (as shown in Fig. 3). The imaginary part (reactance) of the antenna is close to zero in the range of 0.2 up-to 1 THz, leading to almost constant radiation resistance $R_A = 67 \pm 5\ \Omega$. From 1.2 THz to 15 THz, there is an observed empirical roll-off of f^{-3} in the device responsivity. For constant radiation resistance, the theoretical expectation is a f^{-4} roll-off as discussed in [26]. However, the antenna design frequency range ends around 1.5 THz. At higher frequencies, the Terahertz wave couples directly to the metallization of the FET with a strong frequency-dependent coupling coefficient. Furthermore, in reality a variety of other factors, including impedance matching of the antenna, metallization and active section of the device, manufacturing tolerances, bonding wires, and the transition between the active and passive parts of the detector, could result in varied device responses [22]. If considering detector response at 24.9 and 29.8 THz it seems to be f^{-2} roll-off, which might be due to the Seebeck rectification mechanism discussed in [29]. If we consider the entire range of frequencies from 0.2 up-to 29.8 THz, then the overall roll-off of the device is empirically between f^{-2} and f^{-3}. At approximately 30 THz, the background-limited NEP begins to exceed the common electrically or thermally-limited NEP under room-temperature operation.

Optics EXPRESS

Table 1. AlGaAs/GaAs TeraFET detector responsivity and NEP at U_{GS} = 0 V

Frequency (THz)	$\Re_I$ (mA/W)	NEP (nW/$\sqrt{\text{Hz}}$)
0.25	0.368	4.35
0.5	0.586	2.27
1	0.429	4.46
1.2	0.411	4.06
3.08	0.0035	453.64
4.06	0.1566	10.10
4.84	0.0109	145.19
5.56	0.0102	153.87
12.24	0.00039	4013.93
15.35	0.00035	4492.99
24.9	0.0014	1094.96
29.8	0.0017	936.05

Table 2 summarizes the comparison between this work and state-of-the-art available direct detectors operating at room-temperature. While the ZBSD detector is more sensitive than AlGaAs/GaAs TeraFET, the former shows a strong roll-off with f^{-6} [12] whereas the latter decays only with f^{-3}. ZBSD and AlGaAs/GaAs TeraFETs offer a temporal resolution below 10 ps, while other detectors (compared in Table 2) are slower.

Table 2. Comparison of the state-of-the-art direct room-temperature operable THz detectors technologies. We note here that primary criteria for comparison selection is the operational bandwidth of the detectors

Technology	Operation bandwidth (THz)	Minimum NEP	References
AlGaAs/GaAs TeraFET	0.2 to 29.8 THz	2.27 (nW/$\sqrt{\text{Hz}}$) at 0.5 THz	This work
Zero-Bias Schottky diode (ZBSD)	0.2 to 5.56 THz	10 (pW/$\sqrt{\text{Hz}}$) at 0.5 THz	[12]
Si CMOS	0.76 to 4.25 THz	20 (pW/$\sqrt{\text{Hz}}$) at 0.59 THz	[16]
SiGe HBT	0.2 to 1 THz	1.9 (pW/$\sqrt{\text{Hz}}$) at 0.3 THz	[18]
AlGaN/GaN	0.2 to 1.2 THz	25 (pW/$\sqrt{\text{Hz}}$) at 0.5 THz	[19]
Graphene	0.1 to 10 THz	4.3 (nW/$\sqrt{\text{Hz}}$) at 2.8 THz	[20]

5. Conclusions

We have demonstrated that the GaAs TeraFETs can operate in a broad frequency range from 0.2 THz up to 29.8 THz. The maximum current responsivity ($\Re_I$) of 0.59 mA/W is noted at U_{GS} = 0.18 V, signifying the NEP of 2.27 $nW/\sqrt{Hz}$. There is a noticeable empirical roll-off of f^{-3} with respect to frequencies up-to 29.8 THz where the devices show a noise floor of 0.94 $\mu W/\sqrt{Hz}$. The DS detection mechanism is retained over the entire frequency range. The optimum gate bias shifts towards more positive values when increasing the frequency from 1 and 29.8 THz. This detector can be applied not only to high-power ultra-short pulses of FEL but also to other low-power heterodyne sources such as CW PIN-diode photo-mixers. The GaAs FET decays only with f^{-3} in the THz frequency regime, whereas Schottky diodes roll off strongly with f^{-6} [12] in the 1 to 10 THz range. The device's ability to perform over a broad frequency range, albeit with reduced responsivity, highlights its potential for beam diagnostics and alignment applications in high-power accelerator facilities.

Optics EXPRESS

Funding. Bundesministerium für Bildung und Forschung (05K22RD1, 05K22RO1); Deutsche Forschungsgemeinschaft (RO 770/40-1, RO 770/40-2); Hessisches Ministerium für Wissenschaft und Kunst.

Acknowledgments. We are thankful for the cooperation between TU Darmstadt, Darmstadt, Germany and Mittelhessen University of Applied Sciences, Friedberg (Hesse), Germany, for this project. Moreover, we are grateful to the Hesse Ministry of Science and Culture for funding position of Rahul Yadav. We would like to express our profound gratitude to TU Darmstadt's Open Access (OA) funds.

Disclosures. The authors have no conflicts to disclose.

Data availability. Data underlying the results presented in this paper are not publicly available at this time but may be obtained from the authors upon reasonable request.

References

1. A. Rostami, H. Rasooli, and H. Baghban, *Terahertz Technology: Fundamentals and Applications*, Vol. 77 (Springer Science & Business Media, 2011).
2. A. Redo-Sanchez and X. -C. Zhang, "Terahertz Science and Technology Trends," IEEE J. Select. Topics Quantum Electron. **14**(2), 260–269 (2008).
3. I. Hosako, N. Sekine, M. Patrashin, *et al.*, "At the Dawn of a New Era in Terahertz Technology," Proc. IEEE **95**(8), 1611–1623 (2007).
4. G. Carpintero, E. G. Munoz, H. L. Hartnagel, *et al.*, *Semiconductor TeraHertz Technology: Devices and Systems at Room Temperature Operation* (Wiley-IEEE Press, 2015).
5. H. -B. Liu, H. Zhong, N. Karpowicz, *et al.*, "Terahertz Spectroscopy and Imaging for Defense and Security Applications," Proc. IEEE **95**(8), 1514–1527 (2007).
6. D. L. Woolard, J. O. Jensen, and R. J. Hwu, *Terahertz Science and Technology for Military and Security Applications* (World Scientific, 2007).
7. J. Beckmann, H. Spranger, and U. Ewert, "THz Applications for Non-Destructive Testing," in *Far East NDT New Technology & Application Forum* (2017), pp. 272–276.
8. R. Fukasawa, "Terahertz Imaging: Widespread Industrial Application in Non-destructive Inspection and Chemical Analysis," IEEE Trans. Terahertz Sci. Technol. **5**(6), 1121-1127 (2015).
9. S. Zhong, "Progress in terahertz nondestructive testing: A review," Front. Mech. Eng. **14**(3), 273–281 (2019).
10. S. Regensburger, "Large-area and lumped element field-effect transistors for picosecond-scale detection in the Terahertz band and beyond," Ph.D dissertation, Technical University of Darmstadt, Darmstadt, Germany, 2019.
11. S. Regensburger, S. Winnerl, J. M. Klopf, *et al.*, "Picosecond-Scale Terahertz Pulse Characterization With Field-Effect Transistors," IEEE Trans. Terahertz Sci. Technol. **9**(3), 262–271 (2019).
12. R. Yadav, F. Ludwig, F. R. Faridi, *et al.*, "State-of-the-Art Room Temperature Operable Zero-Bias Schottky Diode-Based Terahertz Detector Up to 5.56 THz," Sensors **23**(7), 3469 (2023).
13. R. A. Lewis, "A review of terahertz detectors," J. Phys. D: Appl. Phys. **52**(43), 433001 (2019).
14. F. Simoens, "THz bolometer detectors," in *Physics and Applications of Terahertz Radiation* (Springer, 2013), vol 173.
15. V. V. Parshin, E. A. Serov, G. M. Bubnov, *et al.*, "Terahertz reflectivity of $YBa_2Cu_3O_7$ at cryogenic temperatures," IEEE Trans. Appl. Supercond. **30**(8), 1–5 (2020).
16. M. Bauer, R. Venckevičius, I. Kašalynas, *et al.*, "Antenna-coupled field-effect transistors for multi-spectral terahertz imaging up to 4.25 THz," Opt. Express **22**(16), 19235–19241 (2014).
17. R. Kesselring, A. W. Kälin, and F. K. Kneubühle, "Fast mid-infrared detectors," Infrared Phys. **33**(5), 423–436 (1992).
18. M. Andree, J. Grzyb, R. Jain, *et al.*, "Broadband Modeling, Analysis, and Characterization of SiGe HBT Terahertz Direct Detectors," IEEE Trans. Microw. Theory Techn. **70**(2), 1314–1333 (2022).
19. M. Bauer, A. Rämer, S. A. Chevtchenko, *et al.*, "A High-Sensitivity AlGaN/GaN HEMT Terahertz Detector With Integrated Broadband Bow-Tie Antenna," IEEE Trans. Terahertz Sci. Technol. **9**(4), 430–444 (2019).
20. M. Asgari, E. Riccardi, O. Balci, *et al.*, "Chip-Scalable, Room-Temperature, Zero-Bias, Graphene-Based Terahertz Detectors with Nanosecond Response Time," ACS Nano **15**(11), 17966–17976 (2021).
21. M. Laabs, N. Neumann, B. Green, *et al.*, "On-chip THz spectrometer for bunch compression fingerprinting at fourth-generation light sources," J. Synchrotron Rad. **25**(5), 1509–1513 (2018).
22. S. Preu, S. Kim, R. Verma, *et al.*, "An improved model for non-resonant terahertz detection in field-effect transistors," J. Appl. Phys **111**(2), 024502 (2012).
23. M. Dyakonov and M. Shur, "Shallow water analogy for a ballistic field effect transistor: New mechanism of plasma wave generation by dc current," Phys. Rev. Lett. **71**(15), 2465–2468 (1993).
24. M. Dyakonov and M. Shur, "Detection, mixing, and frequency multiplication of terahertz radiation by two-dimensional electronic fluid," IEEE Trans. Electron Devices **43**(3), 380–387 (1996).
25. F. Ludwig, A. Generalov, J. Holstein, *et al.*, "Terahertz Detection with Graphene FETs: Photothermoelectric and Resistive Self-Mixing Contributions to the Detector Response," ACS Appl. Electron. Mater. **6**(4), 2197–2212 (2024).
26. S. Regensburger, A. K. Mukherjee, S. Schönhuber, *et al.*, "Broadband Terahertz Detection With Zero-Bias Field-Effect Transistors Between 100 GHz and 11.8 THz With a Noise Equivalent Power of 250 pW/$\sqrt{Hz}$ at 0.6 THz," IEEE Trans. Terahertz Sci. Technol. **8**(4), 465–471 (2018).

Optics EXPRESS

27. V. V. Popov, "Terahertz rectification by periodic two-dimensional electron plasma," Appl. Phys. Lett. **102**(25), 253504 (2013).
28. M. M. Aller, "Photonic Terahertz signal analyzers: fully ballistic Terahertz source for a photonic VNA and error analysis of Terahertz time domain spectroscopy of liquids," Ph.D dissertation, Technical University of Darmstadt, Darmstadt, Germany, 2022.
29. S. Regensburger, F. Ludwig, S. Winnerl, *et al.*, "Mapping the slow and fast photoresponse of field-effect transistors to terahertz and infrared radiation," Opt. Express **32**(5), 8447–8458 (2024).

212.201.7.144 {ts '2024-11-15 02:16:57'}